High-Efficiency Asymmetrical Half-Bridge Converter With a New Coupled Inductor Rectifier (CIR)

Jung-Kyu Han, *Student Member, IEEE*, Jong-Woo Kim, *Member, IEEE*, Byoung-Hee Lee, *Member, IEEE*, Jih-Sheng Lai, *Life Fellow, IEEE*, and Gun-Woo Moon, *Member, IEEE*

(Highlighted Paper)

***Abstract*—A conventional asymmetrical half-bridge (AHB) converter is one of the most promising topologies in low-power applications because of the zero-voltage switching (ZVS) of all switches and the small number of components. However, when it operates with an asymmetrical duty ratio, it has a large dc-offset current in the transformer, which increases the size and core loss of the transformer. Moreover, because the dc-offset current decreases ZVS energy for one of the half-bridge switches, it has low efficiency in a light load condition. In addition, because most of the output current is concentrated in high-voltage-rating diodes that have large forward voltage drops, large conduction loss occurs in the secondary rectifier. To solve these problems, a new AHB converter with a coupled inductor rectifier (CIR) is proposed in this paper. By adopting the CIR structure in the AHB converter, the proposed converter not only eliminates the dc-offset current in the transformer, but it also has equalized current stress in the rectifier diodes. As a result, the proposed converter achieves high efficiency in entire load condition, compared to an AHB converter with a full-bridge rectifier. The effectiveness and feasibility are verified with a 250–400 V input and 100 V/200 W output prototype.**

***Index Terms*—Asymmetrical half-bridge (AHB) converter, coupled inductor rectifier (CIR), dc-offset current, high efficiency, zero-voltage switching (ZVS).**

I. Introduction

AN ASYMMETRICAL half-bridge (AHB) converter shown in Fig. 1(a) is one of the most promising topologies for low-power applications, such as TV and LED drivers, because of its small number of components. In addition, all of the primary switches not only have zero-voltage switching (ZVS) capability, but also have clamped voltage stress [1]–[4].

Manuscript received September 21, 2018; revised January 20, 2019; accepted March 7, 2019. Date of publication March 20, 2019; date of current version September 6, 2019. This work was supported by the National Research Foundation of Korea funded by Korea government (MSIP) under Grant 2016R1A2B2010328. Recommended for publication by Associate Editor D. G. Lamar. *(Corresponding author: Gun-Woo Moon.)*

J.-K. Han and G.-W. Moon are with the Department of Electrical Engineering, Korea Advanced Institute of Science and Technology, Daejeon 305-701, South Korea (e-mail:

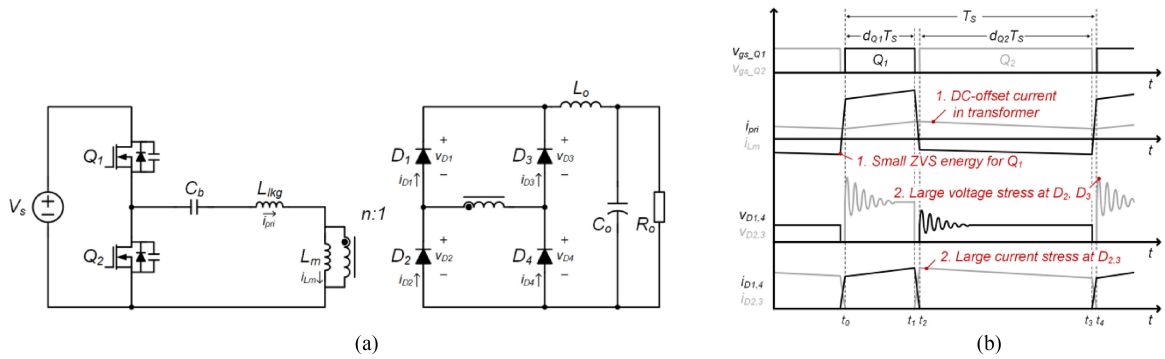

Fig. 1. Conventional AHB converter. (a) Circuit diagram. (b) Key waveforms.

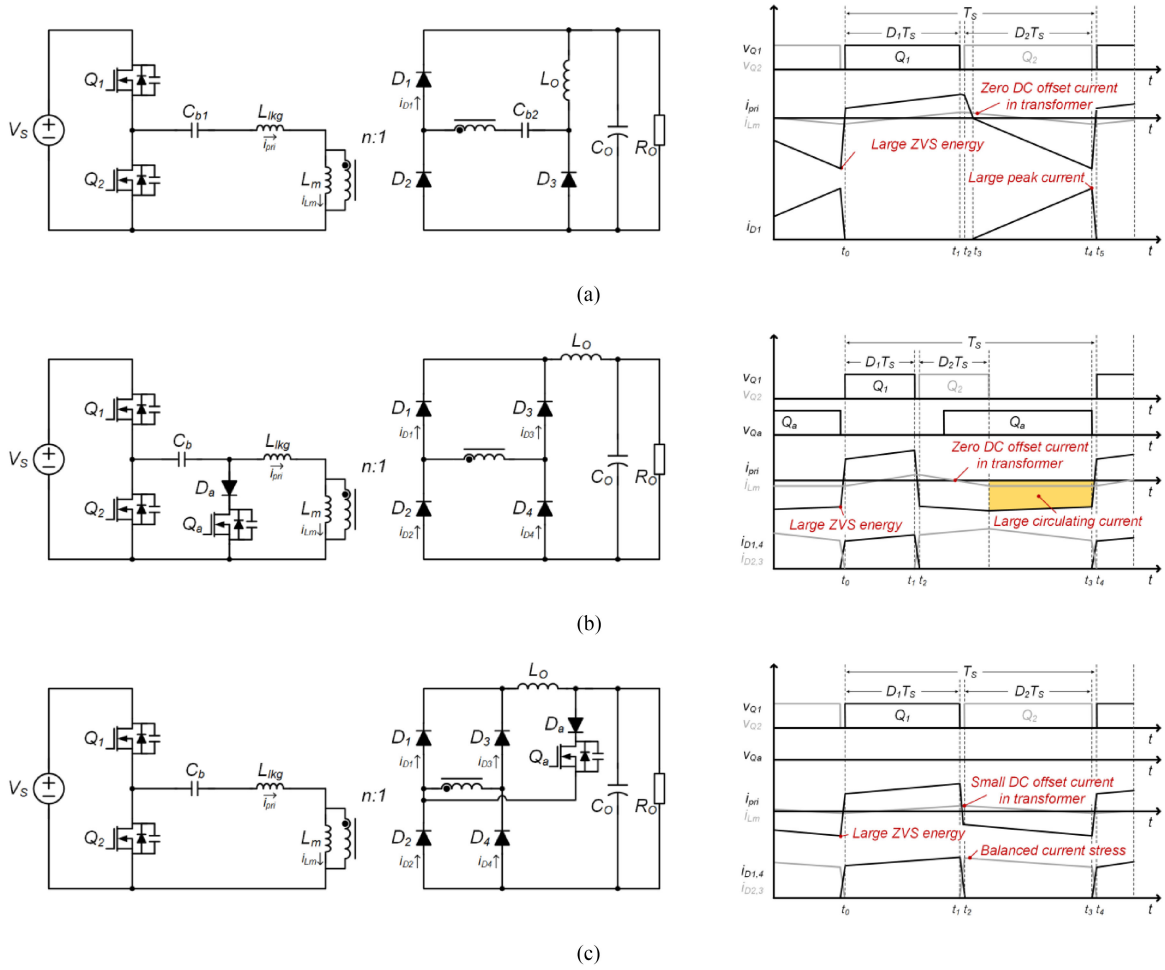

Fig. 2. Recent studies on a conventional AHB converter and its key waveforms. (a) Zero dc-offset AHB converter [20]. (b) DCS HB converter [21]. (c) Boost-integrated AHB converter [22].

shown in Fig. 2(c). Because it can obtain additional voltage gain of the integrated boost converter, it regulates the output voltage with the Q_a when the input voltage is low. Therefore, when the input voltage is high, the additional switch Q_a does not operate and primary switches can operate with large duty ratio regardless of the input voltage range, which solves the problems caused by the wide range of input voltage. However, the additional devices not only increase its cost and complexity, but also cause large conduction loss and switching loss when the input voltage is low. In addition, the output filter has to be increased because it has discontinuous output current when Q_a operates.

Therefore, to solve more simply the aforementioned problems without adding other components, an AHB converter with a new coupled inductor rectifier (CIR) is proposed in this paper. By

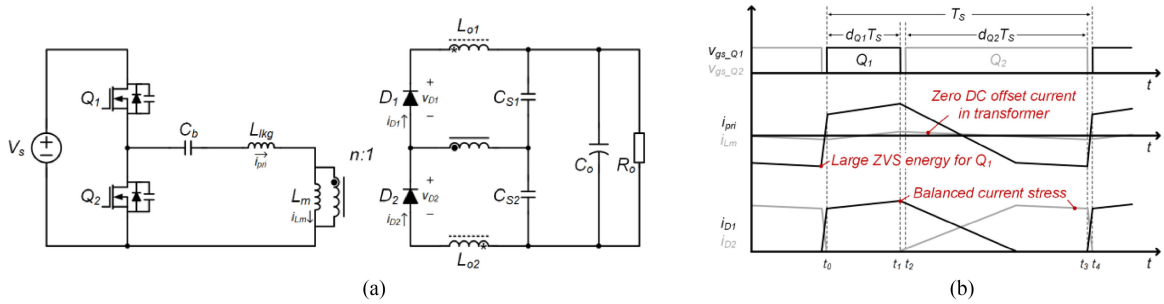

Fig. 3. Proposed AHB converter. (a) Circuit diagram. (b) Key waveforms.

adopting the CIR structure in the AHB converter instead of the full-bridge rectifier (FBR), the proposed converter eliminates the dc-offset current of the transformer, and it has balanced current stress at the rectifier diodes. In addition, it has better ZVS condition for Q_1 because it does not have positive dc-offset current in the transformer. Therefore, the proposed converter achieves high efficiency compared to a conventional AHB converter with FBR.

The remainder of this paper is organized as follows. The concept and operational principles are analyzed in Sections II and III, respectively. In Section IV, the characteristics of the proposed converter are analyzed. A 250–400 V input and 100 V/200 W output prototype was built and tested to verify the effectiveness and feasibility of the proposed converter in Section V. Finally, the conclusions are presented in Section VI.

II. Concept of the Proposed Converter

Fig. 3 shows the proposed AHB converter and its key waveforms. As shown in this figure, the proposed converter has a new rectifier structure using a coupled output inductor while the primary side of the proposed converter and the control method are the same as in the conventional AHB converter. Because the proposed converter does not need additional components or a control method, its cost and complexity are not increased.

The proposed converter has three main advantages by adopting the CIR structure instead of the FBR to the conventional AHB converter. Fig. 4 presents comparison of the characteristics of the each rectifier. In the case of the conventional AHB converter with FBR shown in Fig. 4(a), the rectifier diodes D_1 and D_4 conducted when Q_1 is turned ON and D_2 and D_3 conducted when Q_2 is turned ON. Therefore, the average current flowing through D_1 and D_4 is $d_{Q1}I_o$ during d_{Q1} and the average current flowing through D_2 and D_3 is $(1–d_{Q1})I_o$ during $d_{Q2}(= 1–d_{Q1})$. Because the AHB converter has small d_{Q1} in the nominal state, a large current is concentrated at D_2 and D_3, which has large forward voltage drop V_F and it causes severe conduction loss. In addition, the difference of average current between D_1 and D_2 flows to the secondary winding of the transformer and it is transferred to the primary side. Because the average current of C_b is zero, the transformer has a positive dc-offset current as $(1–2d_{Q1})/n$, and it degrades the transformer design and ZVS condition of Q_1.

However, in the case of the proposed converter shown in Fig. 4(b), the average current flowing through the secondary

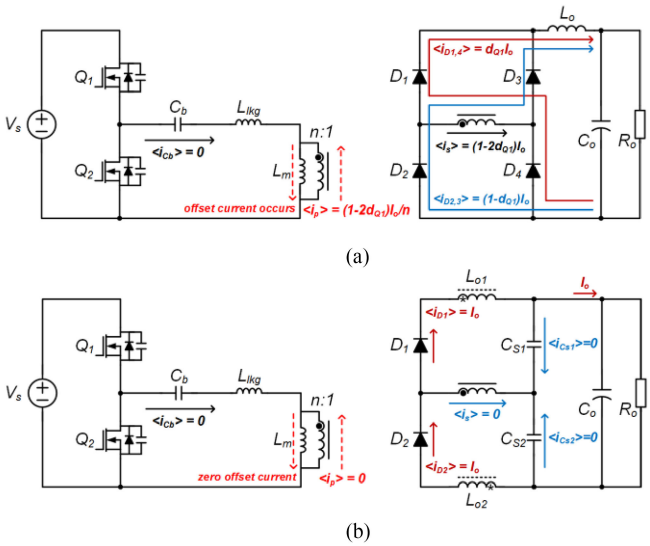

Fig. 4. Characteristics of each rectifier. (a) Conventional AHB converter with FBR. (b) Proposed AHB converter with CIR.

winding of the transformer $< i_s >$ is always zero, because the average current of C_{s1} and C_{s2} is zero. Therefore, the proposed converter does not have dc-offset current, which improves the transformer design and ZVS condition of Q_1. In addition, because $< i_{Cs1} >$, $< i_{Cs2} >$, and $< i_s >$ are zero, D_1 and D_2 have the same current stress, which relieves the conduction loss at the rectifier diodes.

As a result, compared with a conventional AHB converter with FBR, the proposed AHB converter has advantages in transformer design, ZVS operation of Q_1, and current balance between rectifier diodes by adopting the CIR structure, which results in a high efficiency for the entire load condition.

III. Operational Principles

To explain the operational principles of the proposed converter, the current paths and key waveforms are presented in Figs. 5 and 6, respectively. As shown in Fig. 5(a)–(e), the proposed converter has five operating modes and each mode is analyzed in detail. For the simplicity of the analysis, some assumptions are made as follows.

1) All parasitic components except for those specified in Fig. 5 are ignored.

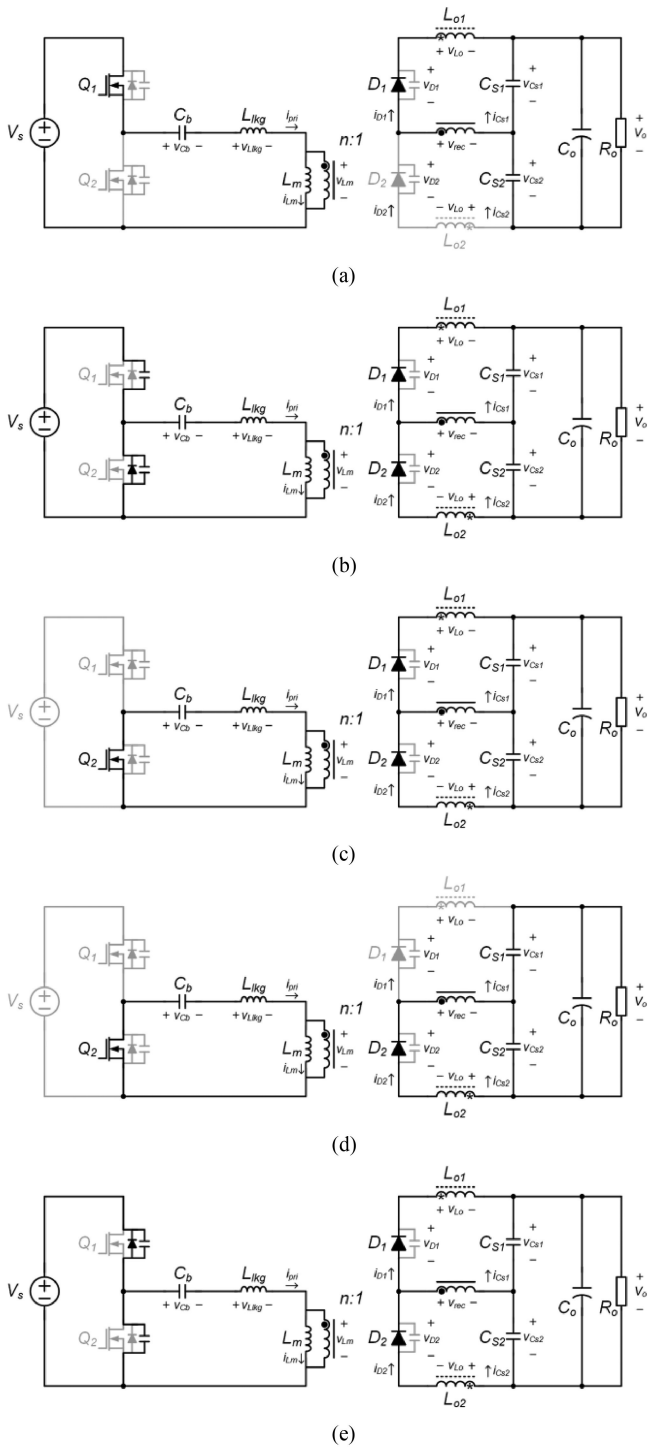

Fig. 5. Current paths of the proposed converter. (a) Mode 1. (b) Mode 2. (c) Mode 3. (d) Mode 4. (e) Mode 5.

2) The magnetizing inductance L_m, the output inductor L_{o1}, and L_{o2} are large enough to be considered as a constant current source during a dead time of the primary switches.
3) The turns ratio of the coupled inductor is 1:1 and it has a large coupling coefficient.
4) The magnetizing inductance is large enough than the leakage inductance.

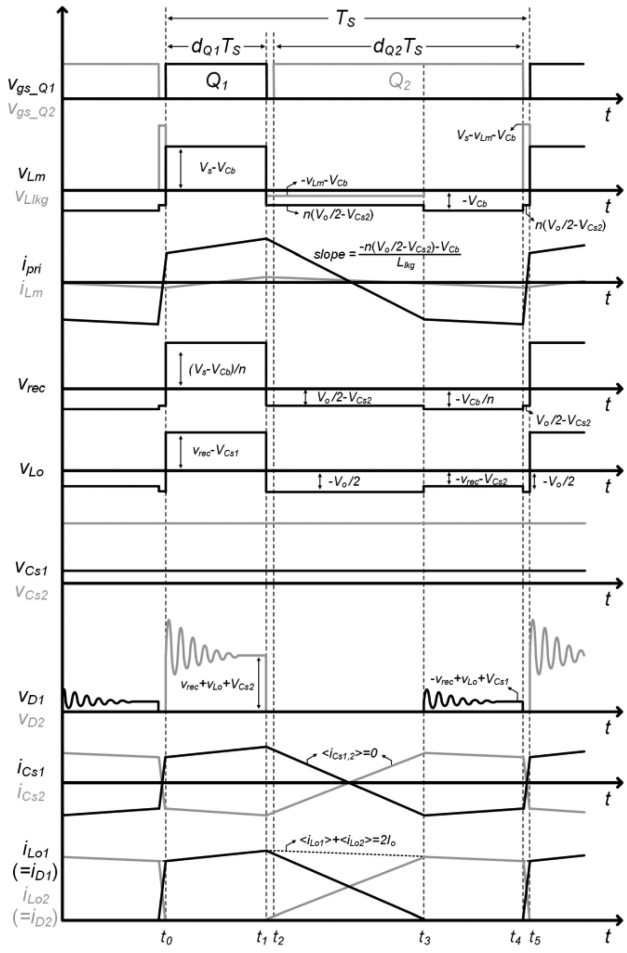

Fig. 6. Key waveforms of the proposed converter.

Mode 1 [t_0–t_1]: Mode 1 starts when the current commutation between D_1 and D_2 is finished. Since the parasitic capacitor of D_2 resonates with primary and secondary leakage inductors, it causes voltage ringing up to $2 \times (V_{\rm rec} + V_{Lo} + V_{Cs2})$. During mode 1, V_s–V_{Cb} is applied to the transformer, and it is transferred to the secondary side of the transformer as $(V_s$–$V_{Cb})/n$. Accordingly, $(V_s$–$V_{Cb})/n$–V_{Cs1} is applied to the output inductor L_{o1} and L_{o1} builds up the output current. The magnetizing current of the transformer $i_{Lm}(t)$, primary current $i_{\rm pri}(t)$, and output inductor current $i_{Lo1}(t)$ are determined as follows:

$$i_{Lm}(t) = i_{Lm}(t_0) + \frac{V_s - V_{Cb}}{L_m}(t - t_0) \tag{1}$$

$$i_{Lo1}(t) = i_{Lo1}(t_0) + \frac{(V_s - V_{Cb})/n - V_{Cs1}}{L_{o1}}(t - t_0) \tag{2}$$

$$i_{\rm pri}(t) = i_{Lm}(t) + \frac{i_{Lo1}(t)}{n}. \tag{3}$$

Mode 2 [t_1–t_2]: Mode 2 starts when Q_1 is turned OFF. Since Q_1 is turned OFF, the current flows through the output capacitor of Q_1. As a result, the output capacitor of Q_1 starts charging, and the output capacitor of Q_2 starts discharging. And, since the output capacitor of Q_2 is discharged, v_{Lm} and $v_{\rm rec}$ start to

decrease. When $v_{\rm rec}$ reaches $V_o/2$–V_{Cs2}, v_{D2} becomes zero, and D_2 conducts. Because both D_1 and D_2 are conducted during mode 2, the voltage across the output inductor is clamped to $-V_o/2$ and $v_{\rm rec}$ is clamped to $V_o/2$–V_{Cs2}. Accordingly, v_{Lm} is clamped to $n(V_o/2$–$V_{Cs2})$ and $-n(V_o/2$–$V_{Cs2})$–V_{Cb} is applied to $L_{\rm lkg}$. Therefore, $i_{\rm pri}$ starts to decrease with a slope of $(-v_{Lm}$–$V_{Cb})/n$ and current commutation occurs between L_{o1} and L_{o2}. Assume that the i_{Lm}, i_{Lo1}, and i_{Lo2} are constant during the dead time, and $i_{\rm pri}$, i_{Lo1}, and i_{Lo2} are determined as follows:

$$i_{\rm pri}(t) = i_{Lm}(t_1) + i_{\rm pri}(t_1) + \frac{-n(V_o/2 - V_{Cs2}) - V_{Cb}}{L_{\rm lkg}}(t - t_1) \quad (4)$$

$$i_{Lo1}(t) = i_{Lo1}(t_1) + \frac{n}{2}\left(\frac{-n(V_o/2 - V_{Cs2}) - V_{Cb}}{L_{\rm lkg}}\right)(t - t_1) \quad (5)$$

$$i_{Lo2}(t) = \frac{n}{2}\left(\frac{n(V_o/2 - V_{Cs2}) + V_{Cb}}{L_{\rm lkg}}\right)(t - t_1). \quad (6)$$

Mode 3 [t_2–t_3]: When Q_2 is turned ON, mode 3 starts. Since the output capacitor of Q_2 is discharged during mode 2, the ZVS of Q_2 can be achieved. And $i_{\rm pri}$ continues to decrease with the same slope as in mode 2 until the current commutation between D_1 and D_2 is ended. Because the output current flows through D_1 and D_2 when Q_2 is turned ON, D_1 and D_2 have balanced current stress, whereas the conventional AHB converter handles the output current with D_2 only when Q_2 is turned ON.

Mode 4 [t_3–t_4]: Mode 4 starts when i_{D1} reaches zero. Because Q_2 is turned ON, V_{Lm} is clamped to $-V_{Cb}$ and $v_{\rm rec}$ is clamped to $-V_{Cb}/n$. During mode 4, L_o demagnetizes the output current with a slope of $(-V_{\rm rec}$–$V_{Cs2})/L_{o2}$. $i_{Lm}(t)$, $i_{\rm pri}(t)$, and $i_{D2}(t)$ are determined as follows:

$$i_{Lm}(t) = i_{Lm}(t_3) + \frac{-V_{Cb}}{L_m}(t - t_3) \quad (7)$$

$$i_{Lo2}(t) = i_{Lo2}(t_3) + \frac{V_{Cb}/n - V_{Cs2}}{L_{o2}}(t - t_3) \quad (8)$$

$$i_{\rm pri}(t) = i_{Lm}(t) + \frac{i_{Lo2}(t)}{n}. \quad (9)$$

Mode 5 [t_4–t_5]: Mode 5 starts when Q_2 is turned OFF. Because the output capacitors of Q_2 and Q_1 start charging and discharging, respectively, V_{Lm} and $V_{\rm rec}$ increase together. When $V_{\rm rec}$ reaches $V_o/2$–V_{Cs2}, v_{D1} becomes zero and D_1 is conducted. Since D_1 and D_2 are conducted as shown in Fig. 5(e), $-V_o/2$ is applied to L_{o1} and L_{o2}, which makes $v_{\rm rec}$ be clamped to $V_o/2$–V_{Cs2}. Accordingly, v_{Lm} is clamped to $n(V_o/2$–$V_{Cs2})$ and V_s–$n(V_o/2$–$V_{Cs2})$–V_{Cb} is applied to $L_{\rm lkg}$. Therefore, $i_{\rm pri}$ starts to increase rapidly with a slope of $(V_s$–v_{Lm}–$V_{Cb})/L_{\rm lkg}$ and current commutation occurs between L_{o1} and L_{o2}. Assume that the i_{Lm}, i_{Lo1}, and i_{Lo2} are constant during the dead time, $i_{\rm pri}$, i_{Lo1}, and i_{Lo2} are determined as follows:

$$i_{\rm pri}(t) = i_{Lm}(t_4) + i_{\rm pri}(t_4) + \frac{V_s - n(V_o/2 - V_{Cs2}) - V_{Cb}}{L_{\rm lkg}}(t - t_4) \quad (10)$$

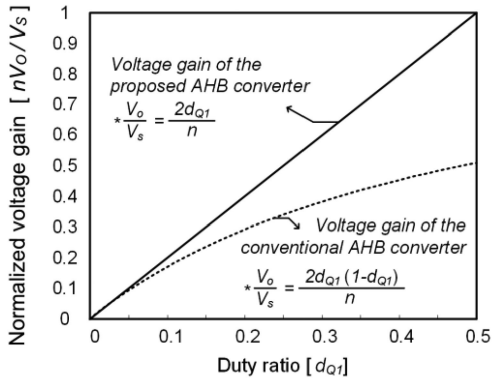

Fig. 7. Normalized voltage gain graphs of the proposed converter and the conventional AHB converter.

$$i_{Lo1}(t) = \frac{n}{2}\left(\frac{V_s - n(V_o/2 - V_{Cs2}) - V_{Cb}}{L_{\rm lkg}}\right)(t - t_4) \quad (11)$$

$$i_{Lo2}(t) = i_{Lo2}(t_4) - \frac{n}{2}\left(\frac{V_s - n(V_o/2 - V_{Cs2}) - V_{Cb}}{L_{\rm lkg}}\right)(t - t_4). \quad (12)$$

IV. Characteristics of the Proposed Converter

A. Voltage Gain

The voltage gain of the proposed converter is obtained by using a voltage–second balance equation to the output inductor. Assuming that a dead time of switches is small enough and duty ratio of the mode 4 is the same as of the mode 2 in Fig. 6, the voltage–second balance equation is obtained as follows:

$$\left(\frac{V_s - V_{Cb}}{n} - V_{Cs1}\right)\cdot d_{Q1} + \left(-\frac{V_o}{2}\right)\cdot(1 - 2d_{Q1}) + \left(\frac{V_{Cb}}{n} - V_o + V_{Cs1}\right)\cdot d_{Q1} = 0 \quad (13)$$

$$\frac{V_o}{V_s} = \frac{2d_{Q1}}{n} \quad (14)$$

where n is the turns ratio of the transformer and $V_{Cs1} + V_{Cs2} = V_o$.

Based on (14), the normalized gain graphs of the proposed converter and the conventional AHB are shown in Fig. 7. Since the proposed converter does not have a $(1$–$d_{Q1})$ term in the numerator, it has a linear voltage gain which is two times larger than that of the conventional AHB converter when d_{Q1} is 0.5. The turns ratio *n* of the proposed converter and the conventional AHB converter is designed as 2.5 and 1.25 in ideal case with a 250–400 V input voltage and 100 V output voltage specification. In practice, the turns ratio is slightly reduced because of the duty-cycle loss.

B. Voltage Gain

The ZVS condition of the primary switches is analyzed in detail with Fig. 8. As shown in the figure, when Q_1 is turned OFF at t_1, $i_{\rm pri}$ starts to charge/discharge an output capacitor

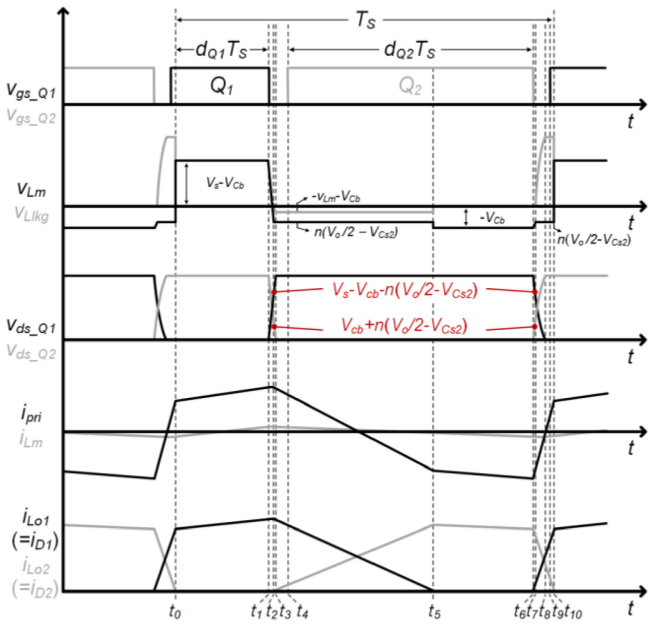

Fig. 8. ZVS operation of the proposed converter.

of Q_1 and Q_2. Accordingly, v_{Lm} decreases until it reaches to $n(V_o/2–V_{Cs2})$ at t_2. Because D_1 and D_2 are turned ON at t_2, v_{Lm} is clamped to $n(V_o/2–V_{Cs2})$ and the drain–source voltage v_{ds_Q1} and v_{ds_Q2} are charged/discharged by $L_{\rm lkg}$. Because a general equation between the magnetic and capacitive elements is expressed as $\frac{1}{2}LI^2 = \frac{1}{2}CV^2$, the ZVS condition of Q_2 can be determined as follows:

$$\frac{1}{2}L_{\rm lkg}i_{\rm pri}(t_2)^2 = \frac{1}{2}L_{\rm lkg}\left(\frac{2I_o}{n}\right)^2 \geq \left(\frac{1}{2}C_{oss}{V_s}^2 - \frac{1}{2}C_{oss}(V_s - V_{Cb} - n(V_o/2 - V_{Cs2}))^2\right) + \frac{1}{2}C_{oss}(V_{Cb} + n(V_o/2 - V_{Cs2}))^2 = C_{oss}V_s\frac{nV_{Cs1}}{2d_{Q1}} \quad (15)$$

where C_{oss} is the output capacitance of the primary switches.

And when Q_2 is turned OFF at t_6, $i_{\rm pri}$ starts to charge/discharge an output capacitor of Q_2 and Q_1 until v_{Lm} decreases to $n(V_o/2–V_{Cs2})$. Because v_{Lm} is clamped to $n(V_o/2–V_{Cs2})$ from t_7, v_{ds_Q1} and v_{ds_Q2} are charged/discharge by $L_{\rm lkg}$. The ZVS condition of Q_1 is obtained as follows:

$$\frac{1}{2}L_{\rm lkg}i_{\rm pri}(t_7)^2 = \frac{1}{2}L_{\rm lkg}\left(\frac{2I_o}{n}\right)^2 \geq \frac{1}{2}C_{oss}(V_s - V_{Cb} - n(V_o/2 - V_{Cs2}))^2 + \left(\frac{1}{2}C_{oss}{V_s}^2 - \frac{1}{2}C_{oss}\left(V_{Cb} + n(V_o/2 - V_{Cs2})\right)^2\right) = C_{oss}V_s\left(V_s - \frac{nV_{Cs1}}{2d_{Q1}}\right). \quad (16)$$

Since the required ZVS energy for Q_1 is much larger than that of Q_2, $L_{\rm lkg}$ is designed to achieve the ZVS of Q_1 similar with the conventional AHB converter. Using (16) and (17), which is the ZVS condition of Q_1 in the conventional AHB converter [11], the required $L_{\rm lkg}$ of both converters are drawn as shown in Fig. 9

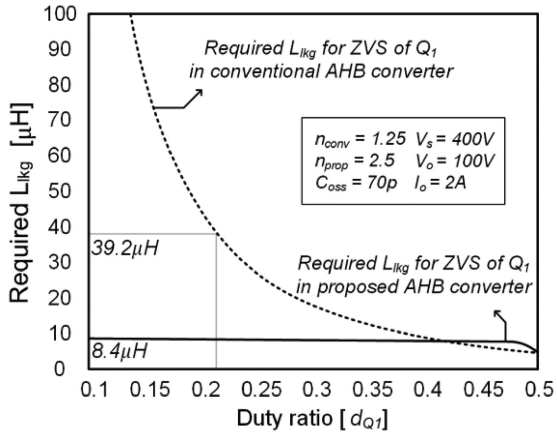

Fig. 9. Required leakage inductance for the ZVS of Q_1.

$$\frac{1}{2}L_{\rm lkg}\left(-\frac{2d_{Q1}I_o}{n}\right)^2 \geq C_{oss}\left(1 - d_{Q1}\right){V_s}^2. \quad (17)$$

As shown in the figure, the conventional AHB converter requires large $L_{\rm lkg}$ at small duty ratio because it has small negative current due to the positive offset current in the transformer. On the other hand, the proposed converter easily achieves the ZVS of Q_1 even at the small duty ratio since it does not have the offset current.

C. Voltage and Current Stresses of the Secondary Rectifier

The voltage stresses of the secondary rectifier can be determined with Figs. 5 and 6. Assuming that $(t_1–t_0)T_s = d_{Q1\_A}T_s$, $(t_3–t_1)T_s = d_{Q2\_A}T_s$, $(t_4–t_3)T_s = d_{Q2\_B}T_s$, and $(t_5–t_4)T_s = d_{Q1\_B}T_s$ in Fig. 5, the following equations are obtained using a current slope of $i_{\rm pri}$ during a dead time:

$$\frac{n(V_o/2 - V_{Cs2}) + V_{Cb}}{L_{\rm lkg}}(d_{Q2\_A})T_s = \frac{V_s - n(V_o/2 - V_{Cs2}) - V_{Cb}}{L_{\rm lkg}}(d_{Q1\_B})T_s = \frac{4I_o}{n} \quad (18)$$

where $d_{Q1\_A} + d_{Q1\_B} + d_{Q2\_A} + d_{Q2\_B} = 1$. And, assuming that $d_{Q1\_A} = d_{Q2\_B}$, following equations can be obtained using (18):

$$V_{Cs1} = \frac{4I_oL_{\rm lkg}}{n^2d_{Q2\_A}T_s} \quad (19)$$

$$V_{Cs2} = V_o - \frac{4I_oL_{\rm lkg}}{n^2d_{Q2\_A}T_s} \quad (20)$$

$$\frac{Vs}{Vs - n(V_o/2 - V_{Cs2})}d_{Q2\_A} + 2d_{Q2\_B} = 1. \quad (21)$$

Therefore, V_{Cs1} and V_{Cs2} can be drawn as shown in Fig. 10 based on (19) and (21) according to the duty variation of $d_{Q2\_A} + d_{Q2\_B}$.

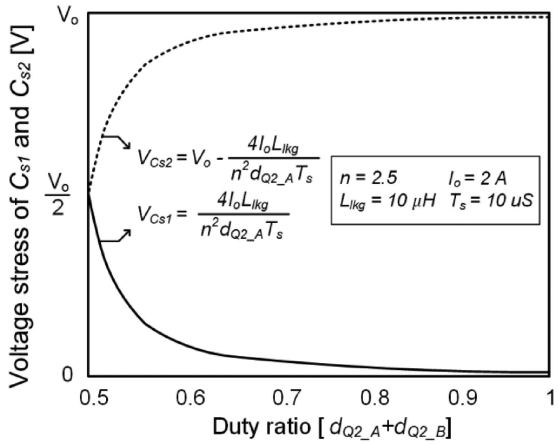

Fig. 10. Voltage stresses of the secondary capacitors C_{s1} and C_{s2}.

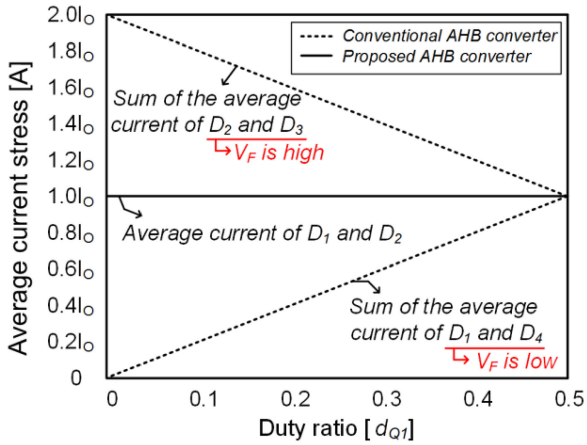

Fig. 11. Current stresses of the rectifier diodes at the conventional AHB converter and the proposed converter.

As shown in the figure, $V_{Cs1} = V_{Cs2} = V_o/2$ when $d_{Q2\_A} + d_{Q2\_B} = 0.5$, which means the maximum duty-ratio of the converter. And, as $d_{Q2\_A} + d_{Q2\_B}$ becomes larger, V_{Cs1} starts to decrease and V_{Cs2} starts to increase.

The voltage stresses of D_1 and D_2 are also obtained with Figs. 5 and 6 as follows:

$$V_{D1} = -v_{\rm rec} + v_{Lo} + V_{Cs1} = 2V_{Cs1} \tag{22}$$

$$V_{D2} = v_{\rm rec} + v_{Lo} + V_{Cs2} = \frac{2V_s}{n} - 2V_{Cs1}. \tag{23}$$

Since V_{Cs1} has maximum voltage stress as $V_o/2$ at $d_{Q2\_A} + d_{Q2\_B} = 0.5$, V_{D1} and V_{D2} are same as V_o when $d_{Q2\_A} + d_{Q2\_B} = 0.5$. And, when $d_{Q1\_A} + d_{Q1\_A} < 0.5$, V_{D2} is larger than V_{D1} similar to that of the conventional AHB converter.

Fig. 11 shows the average current stresses of the rectifier diodes in the conventional AHB converter and the proposed converter. In the conventional AHB converter, the average current of D_2 and D_3 is larger than that of D_1 and D_4. However, since D_2 and D_3 have much larger voltage stress, it causes large conduction loss. On the other hand, the proposed converter has same current stress at D_1 and D_2 although D_1 has larger voltage stress than D_2. Therefore, the proposed converter reduces conduction loss at the rectifier diode.

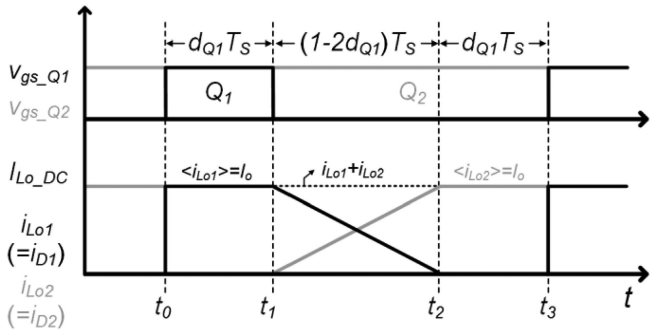

Fig. 12. Output inductor current i_{Lo1} and i_{Lo2}.

D. Coupled Inductor Design

The proposed converter uses a coupled inductor as an output inductor to construct the CIR. There are guidelines to design the output filters for the CIR structure. First, the turns ratio of the coupled inductor should be designed as 1:1. Although the turns ratio of the coupled inductor can be designed as asymmetric, the asymmetric turns ratio causes a biased voltage and current stresses at the rectifier didoes.

Second, the maximum flux density $B_{\max}$ of the inductor core should be designed by taking into consideration the dc-offset current I_{Lo_DC} of i_{Lo1} and i_{Lo2}. Fig. 12 shows the current flowing through the coupled inductor. Because the average current of D_1 and D_2 is I_o as shown in Fig. 4(b), I_{Lo_DC} is determined as the following equation, assuming that the ripple current and duty-cycle loss are ignored and $(t_0 \sim t_1)\, T_s = (t_2 \sim t_3) T_s$:

$$\frac{1}{2}\left(d_{Q1} + (1 - d_{Q1})\right) I_{Lo\_DC} = I_o \tag{24}$$

$$I_{Lo\_DC} = 2I_o. \tag{25}$$

Third, the windings of the coupled inductor should be selected by taking into consideration the rms value of i_{Lo1} and i_{Lo2}. The rms value can be calculated using Fig. 12 as follows:

$$i_{Lo1\_\rm RMS} = i_{Lo2\_\rm RMS} = \sqrt{\int_0^{t_1} I_{Lo\_DC}^2 dt + \int_{t_1}^{t_2} \left(-\frac{I_{Lo\_DC}}{1-2d_{Q1}} t + \frac{1-d_{Q1}}{1-2d_{Q1}} I_{Lo\_DC}\right)^2 dt}. \tag{26}$$

Combining (26) with (25) gives the rms current as follows:

$$i_{Lo1\_\rm RMS} = i_{Lo2\_\rm RMS} = 2I_o\sqrt{\frac{d_{Q1}+1}{3}}. \tag{27}$$

V. Experimental Results

The effectiveness and feasibility of the proposed converter were compared to the conventional AHB converter with FBR in 250–400 V input and 100 V/200 W output specifications. Design examples of the prototype converters are listed in Table I. As shown in the table, the proposed converter is designed to use a small transformer core, because the proposed converter does not have a dc-offset current in the transformer. In addition, since it has larger ZVS energy, it does not require an external

TABLE I
DESIGN EXAMPLES OF THE PROTOTYPE CONVERTERS

	Conventional AHB converter with FBR	Proposed AHB converter with CIR
Primary switches (Q_1, Q_2)	IPP60R600 (v_{ds_max}=600 V, $R_{ds,on}$=600 mΩ)	
Transformer (L_m, turns-ratio, volume)	PQ3220 (400 μH, 24:24, 9440 mm^3)	PQ2620 (400 μH, 22:10, 5490 mm^3)
Leakage inductance of transformer (L_{lkg_tr})	5 μH	7 μH
External inductor (L_{lkg_ext}, volume)	PQ2016 (20 μH, 2330 mm^3)	–
ZVS range of Q_1	At 100% load condition	At 100% load condition
ZVS range of Q_2	Entire load condition	Entire load condition
Secondary rectifier diode (D_1)	MBR40250G (V_R=250 V, V_F=0.62 V)	MBR40250G (V_R=250 V, V_F=0.62 V)
Secondary rectifier diode (D_2)	SCS210AM (V_R=650 V, V_F=1.4 V)	SCS210AM (V_R=650 V, V_F=1.4 V)
Secondary rectifier diode (D_3)	MBR40250G (V_R=250 V, V_F=0.62 V)	–
Secondary rectifier diode (D_4)	SCS210AM (V_R=650 V, V_F=1.4 V)	–
Secondary rectifier capacitor (C_{s1}) (Voltage rating, capacitance)	–	160BXW100MEFR10X25 * 2EA (160 V_{DC}, 100 μH)
Secondary rectifier capacitor (C_{s2}) (Voltage rating, capacitance)	–	160BXW100MEFR10X25 * 2EA (160 V_{DC}, 100 μH)
Output inductor (L_O, wire diameter, volume)	PQ2620 (400 μH, 0.1 Φ*40, 5490 mm^3)	PQ3220 (300 μH, 0.1 Φ*40 2ea, 9440 mm^3)

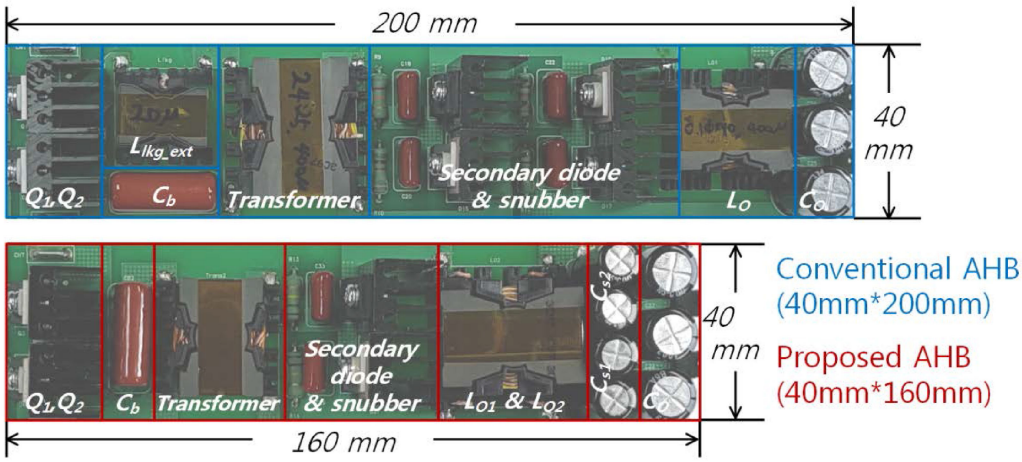

Fig. 13. Picture of the prototype converters.

inductor to achieve the ZVS of Q_1. The sum of $L_{\rm lkg\_tr}$ and $L_{\rm lkg\_ext}$ is expressed as $L_{\rm lkg}$ and two prototype converters have same ZVS energy although they have different $L_{\rm lkg}$. However, in the case of the output inductor, the proposed AHB converter uses larger inductor core since it requires larger winding area to make coupled inductor. Finally, the proposed converter adopts secondary capacitors C_{s1} and C_{s2} to the secondary side instead of D_3 and D_4.

Fig. 13 shows the prototypes of the conventional AHB converter and the proposed AHB converter. Since the proposed converter has larger ZVS energy than the conventional AHB converter, it does not require an external inductor for ZVS. In the case of the transformer and the output inductor, the proposed converter has smaller transformer size due to zero dc-offset current while it uses larger output inductor size due to large winding area of the coupled inductor. And, the proposed converter adopts secondary capacitors for C_{s1} and C_{s2} instead of D_3 and D_4.

Table II shows the cost comparison between the conventional AHB converter and the proposed converter. As shown in the table, the proposed converter has low cost in the primary side since it not only uses small transformer core, but also does not use an external inductor. In the case of the secondary side, the proposed converter has high cost in the output inductor due to large core size. However, because the secondary side capacitors are cheaper than the active devices, it reduces the cost of the

TABLE II
COST COMPARISON OF THE PROTOTYPE CONVERTERS

	Conventional AHB converter	Proposed AHB converter
Primary side	[Transformer] PQ3220 = $ 1.86 [External inductor] PQ2016 = $ 0.60	[Transformer] PQ2620 = $ 1.20
Secondary side	[D_1, D_3] MBR40250G = $ 0.81 EA [D_2, D_4] SCS210AM = $ 2.65 EA [Output inductor] PQ2620 = $ 1.20	[D_1] MBR40250G = $ 0.81 [D_2] SCS210AM = $ 2.65 [C_{s1}, C_{s2}] 160BXW100MEFR10X25 = $ 0.45 EA [Output inductor] PQ3220 = $ 1.86
Total cost	$ 10.58	$ 8.32

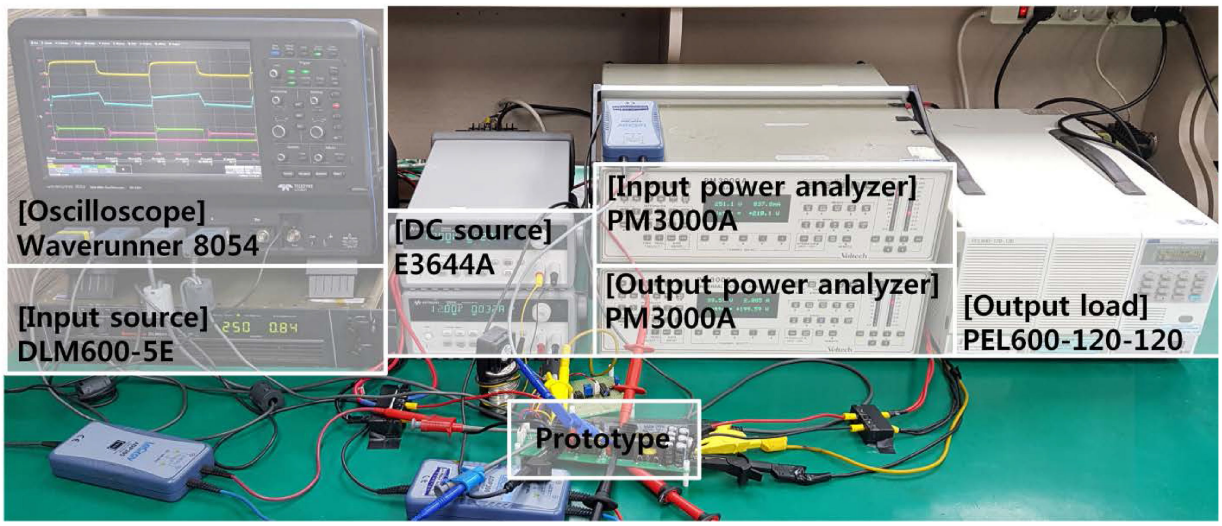

Fig. 14. Picture of the experimental setup.

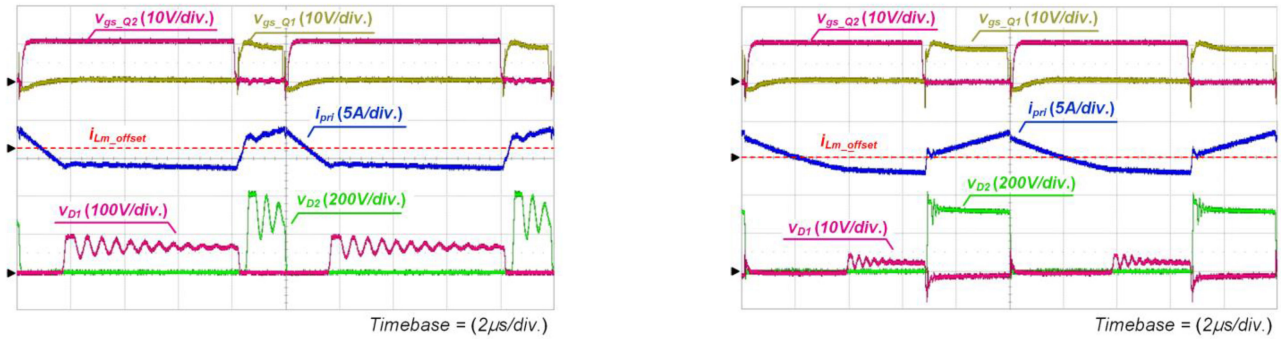

(a) (b)

Fig. 15. Key waveforms of the prototype converters at 100% load condition. (a) Conventional AHB converter. (b) Proposed AHB converter.

secondary side. As a result, the total cost of the proposed converter is reduced compared with the conventional AHB converter.

Fig. 14 shows the picture of the experimental setup and the Table III shows the detailed information. As shown in figure and table, the input source is DLM600-5E, which is a 3000-W dc power supply, and the electric load PEL 600-120-120 is used for the output load. Both input power and output power are analyzed with PM3000A.

Fig. 15 shows the key waveforms of the prototype converters at the 100% load condition. As shown in Fig. 15(a), the conventional AHB converter has a large dc-offset current in the transformer. Since the primary current is biased to positive direction, it has small negative current which degrades a ZVS condition for Q_1. On the other hand, as shown in Fig. 15(b), the proposed converter does not have a dc-offset current in the transformer and it has large negative current compared to the conventional AHB converter. In addition, since the proposed converter

TABLE III
INSTRUMENTS DETAILS

	Model	Remark
Power analyzer for primary side	PM3000A universal power analyzer	Accuracy Voltage : ±0.05% Current : ±0.05%
Power analyzer for secondary side	PM3000A universal power analyzer	Accuracy Voltage : ±0.05% Current : ±0.05%
Input power supply	DLM600-5E	3000W [600V/5A] DC power supply
Output load	PEL 600-120-120	600W [120V/120A] programmable electric load
DC power supply for IC	E3644A	80W [8V/8A or 20V/4A] DC power supply
Oscilloscope	Waverunner 8054	500MHz, 20 GS/s oscilloscope

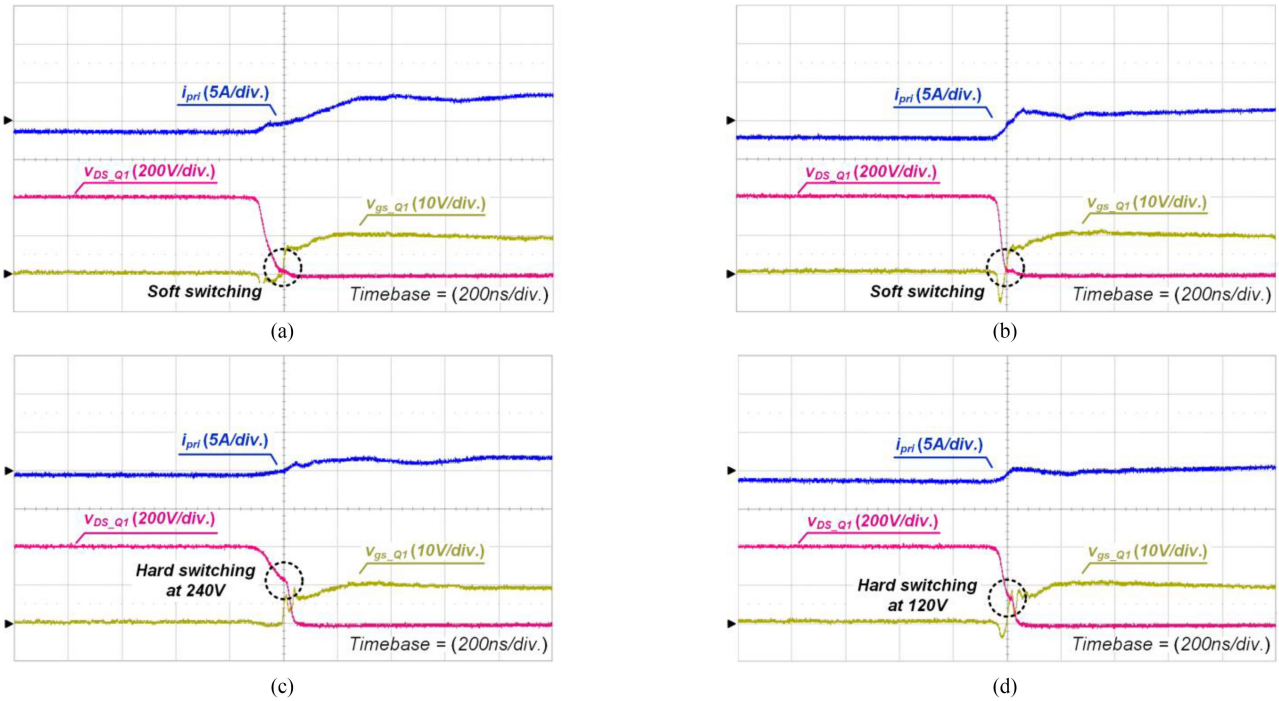

Fig. 16. ZVS waveforms for Q_1 of the prototype converters. (a) Conventional AHB converter at 100% load condition. (b) Proposed converter at 100% load condition. (c) Conventional AHB converter at 50% load condition. (d) Proposed converter at 50% load condition.

uses small $L_{\rm lkg}$, it has small voltage ringing in the rectifier diodes.

Fig. 16 shows the ZVS waveforms of Q_1 of the prototype converters. Fig. 16(a) and (b) show the ZVS waveforms at the 100% load condition and Fig. 16(c) and (d) show the ZVS waveforms at the 50% load condition. As shown in Fig. 16(a) and (b), both converters achieve the ZVS of Q_1 at 100% load condition even though the proposed converter has small $L_{\rm lkg}$ since it has large negative current. And, when the output load decreases, both converters start to do hard switching because the ZVS energy decreases. However, as shown in Fig. 16(c) and (d), the proposed converter turns ON Q_1 at lower V_{ds_Q1} than that of the conventional AHB converter even it has small $L_{\rm lkg}$, which significantly reduces the switching loss.

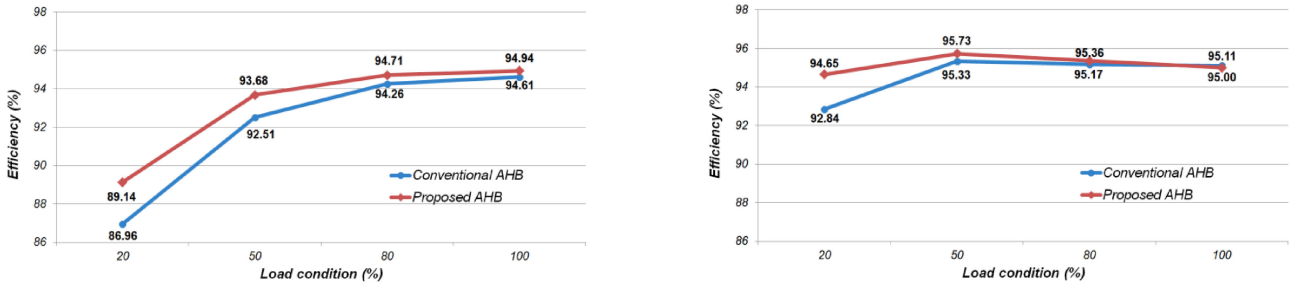

(a) (b)

Fig. 17. Measured efficiency of the prototype converters. (a) $V_S = 400$ V and (b) $V_S = 250$ V.

Fig. 17 shows the measured efficiency of the prototype converters in 250–400 V input voltage and 100 V/200 W output specifications. Because the proposed converter does not have a dc-offset current in the transformer, it not only reduces the size of the transformer, but also does not require an external inductor to achieve the ZVS. Although the proposed converter does not use the external inductor, it has small switching loss in light-load condition, which results in higher efficiency than the conventional AHB converter. In addition, since the proposed converter has balanced current stress at rectifier diodes when the switches operate with asymmetrical duty ratio, it relieves the conduction loss of the high-voltage-rating diode. As a result, the proposed converter achieves high efficiency than the conventional AHB converter.

VI. Conclusion

In this paper, a new AHB converter with a CIR structure is proposed. By adopting the CIR structure to the conventional AHB converter, the proposed converter eliminates the dc-offset current in the transformer, which reduces the size of the transformer and improves the ZVS condition for Q_1. In addition, the two rectifier diodes have the same current stress even in the asymmetrical duty ratio, which reduces conduction loss in high-voltage-rating diode. As a result, the proposed converter achieves higher efficiency than the conventional AHB converter with FBR. Furthermore, because the proposed converter does not need additional components and a control method, its cost and complexity are not increased. Consequently, the proposed converter will be a good candidate for low-power and wide input voltage range applications.

References

[1] H.-S. Lee, H.-J. Choe, S.-H. Ham, and B. Kang, "High-Efficiency asymmetric forward-flyback converter for wide output power range," *IEEE Trans. Power Electron.*, vol. 32, no. 1, pp. 433–440, Jan. 2017.

[2] M. Arias, M. F. Diaz, D. G. Lamar, F. M. F. Linera, and J. Sebastian, "Small-signal and large-signal analysis of the two-transformer asymmetrical half-bridge converter operating in continuous conduction mode," *IEEE Trans. Power Electron.*, vol. 29, no. 7, pp. 3547–3562, Jul. 2014.

[3] W. Li, Y. He, X. He, Y. Sun, and F. Wang, "Series asymmetrical half-bridge converters with voltage autobalance for high input-voltage applications," *IEEE Trans. Power Electron.*, vol. 28, no. 8, pp. 3665–3674, Aug. 2013.

[4] M. Arias, M. F. Diaz, D. G. Lamar, D. Balocco, A. A. Diallo, and J. Sebastian, "High-efficiency asymmetrical half-bridge converter without electrolytic capacitor for low-output-voltage AC–DC LED drivers," *IEEE Trans. Power Electron.*, vol. 28, no. 5, pp. 2539–2550, May 2013.

[5] M. Arias, M. F. Diaz, J. E. R. Cadierno, D. G. Lamar, and J. Sebastian, "Digital implementation of the feedforward loop of the asymmetrical half-bridge converter for LED lighting applications," *IEEE J. Emerg. Sel. Topics Power Electron.*, vol. 3, no. 3, pp. 2539–2550, Sep. 2015.

[6] Y.-S. Lai, Z.-J. Su, and W.-S. Chen, "New hybrid control technique to improve light load efficiency while meeting the hold-up time requirement for two-stage server power," *IEEE Trans. Power Electron.*, vol. 29, no. 9, pp. 4763–4775, Sep. 2014.

[7] H. Wang, H. S.-H. Chung, and W. Liu, "Use of a series voltage compensator for reduction of the DC-link capacitance in a capacitor-supported system," *IEEE Trans. Power Electron.*, vol. 29, no. 3, pp. 1163–1175, Mar. 2014.

[8] J.-W. Kim and G.-W. Moon, "A New LLC series resonant converter with a narrow switching frequency variation and reduced conduction losses," *IEEE Trans. Power Electron.*, vol. 29, no. 8, pp. 4278–4287, Aug. 2014.

[9] R. Kathiresan, P. Das, T. Reindl, and S. K. Panda, "A novel ZVS DC–DC full-bridge converter with hold-up time operation," *IEEE Trans. Ind. Electron.*, vol. 64, no. 6, pp. 4491–4500, Jun. 2017.

[10] J.-B. Lee, J.-K. Kim, J.-H. Kim, J.-I. Baek, and G.-W. Moon, "A high-efficiency PFM half-bridge converter utilizing a half-bridge LLC converter under light load conditions," *IEEE Trans. Power Electron.*, vol. 30, no. 9, pp. 4931–4942, Sep. 2015.

[11] M.-H. Park, C.-O. Yeon, J.-S. Park, C.-Y. Lim, J.-K. Han, and G.-W. Moon, "Wide-Range ZVS asymmetric half-bridge converter with clamping switches for small DC-offset current," in *Proc. IEEE Int. Power Electron. Motion Control Conf.*, May 2016, pp. 2262–2269.

[12] K.-M. Cho, W.-S. Oh, K.-W. Lee, and G.-W. Moon, "A new half bridge converter for the personal computer power supply," in *Proc. IEEE Power Electron. Spec. Conf.*, Aug. 2008, vol. 28, no. 5, pp. 986–991.

[13] S. Chakraborty and S. Chattopadhyay, "An improved asymmetric half-bridge converter with zero DC-offset of magnetizing current," in *Proc. IEEE Appl. Power Electron. Conf. Expo.*, Mar. 2015, vol. 28, no. 5, pp. 1–8.

[14] M. Arias, D. G. Lamar, F. F. Linera, D. Balocco, A. A. Diallo, and J. Sebastian, "Design of a soft-switching asymmetrical half-bridge converter as second stage of an LED driver for street lighting application," *IEEE Trans. Power Electron.*, vol. 27, no. 3, pp. 1608–1621, Mar. 2012.

[15] J.-I. Baek, J.-K. Kim, J.-B. Lee, H.-S. Youn, and G.-W. Moon, "Integrated asymmetrical half-bridge zeta (AHBZ) converter for DC/DC stage of LED driver with wide output voltage range and low output current," *IEEE Trans. Ind. Electron.*, vol. 62, no. 12, pp. 7489–7498, Dec. 2015.

[16] J.-B. Lee, J.-K. Kim, J.-H. Kim, J.-I. Baek, and G.-W. Moon, "A high-efficiency PFM half-bridge converter utilizing a half-bridge LLC converter under light load conditions," *IEEE Trans. Power Electron.*, vol. 30, no. 9, pp. 4931–4942, Sep. 2015.

[17] C.-O. Yeon, J.-B. Lee, I.-O. Lee, and G.-W. Moon, "Wide ZVS range asymmetric half-bridge converter with clamp switch and diode for high conversion efficiency," *IEEE Trans. Ind. Electron.*, vol. 63, no. 5, pp. 2862–2870, May 2016.

[18] C. Yao, X. Ruan, X. Wang, and C. K. Tse, "Isolated buck-boost DC/DC converters suitable for wide input-voltage range," *IEEE Trans. Power Electron.*, vol. 26, no. 9, pp. 2599–2613, Sep. 2011.

[19] J.-B. Lee, K.-B. Park, J.-K. Kim, H.-S. Youn, and G.-W. Moon, "A new center-tapped half-bridge zeta converter with small transformer DC-offset current and low voltage stress," *IEEE Trans. Power Electron.*, vol. 30, no. 12, pp. 6593–6603, Dec. 2015.

[20] I.-O. Lee and G.-W. Moon, "A new asymmetrical half-bridge converter with zero DC-offset current in transformer," *IEEE Trans. Power Electron.*, vol. 28, no. 5, pp. 2297–2306, May 2013.
[21] H. Mao, J. Abu-Qahouq, S. Luo, and I. Batarseh, "Zero-voltage-switching half-bridge DC–DC converter with modified PWM control method," *IEEE Trans. Power Electron.*, vol. 19, no. 4, pp. 947–958, Jul. 2004.
[22] J.-K. Han, J.-W. Kim, and G.-W. Moon, "A high-efficiency asymmetrical half-bridge converter with integrated boost converter in secondary rectifier," *IEEE Trans. Power Electron.*, vol. 32, no. 11, pp. 8237–8242, Nov. 2017.

Jung-Kyu Han (S'16) was born in South Korea, in 1991. He received the B.S. and M.S. degrees in electrical engineering from the Korea Advanced Institute of Science and Technology (KAIST), Daejeon, South Korea, in 2014 and 2016, respectively. He is currently working toward the Ph.D. degree with KAIST.

His research interests include dc–dc converters, power-factor-correction ac–dc converters, digital control, server power system, and onboard charger for electric vehicles.

Jong-Woo Kim (S'13–M'16) received the B.S., M.S., and Ph.D. degrees in electrical engineering from the Korea Advanced Institute of Science and Technology (KAIST), Daejeon, South Korea, in 2010, 2012, and 2016, respectively.

He is currently a Postdoctoral Associate with Virginia Tech, Blacksburg, VA, USA. His research interests include high-efficiency and high-power-density converters and their analog/digital control.

Byoung-Hee Lee (S'07–M'12) received the B.S., M.S., and Ph.D. degrees from the Korea Advanced Institute of Science and Technology (KAIST), Daejeon, South Korea, in 2005, 2008, and 2012, respectively.

From 2012 to 2015, he was a Senior Researcher with Samsung Electronics, Suwon, South Korea. Since 2015, he has been an Assistant Professor with the Department of Electronics and Control Engineering, Hanbat National University, Daejeon. His current research interests include the design of power converters, wireless power transfer systems, power systems for railway cars, and battery management systems.

Prof. Lee is currently an Associate Editor for the *Journal of Power Electronics*.

Jih-Sheng (Jason) Lai (S'85–M'89–SM'93–F'07–LF'19) received the M.S. and Ph.D. degrees in electrical engineering from The University of Tennessee, Knoxville, TN, USA, in 1985 and 1989, respectively.

In 1989, he joined the Electric Power Research Institute (EPRI) Power Electronics Applications Center, where he managed EPRI-sponsored power electronics research projects. In 1993, he then joined the Oak Ridge National Laboratory as a Power Electronics Lead Scientist, where he initiated a high-power electronics program and developed several novel high-power converters including multilevel converters and soft-switching inverters. In 1996, he joined Virginia Polytechnic Institute and State University, Blacksburg, VA, USA, where he is currently the James S. Tucker Professor with the Electrical and Computer Engineering Department and the Director of Future Energy Electronics Center. He authored or coauthored more than 430 refereed technical papers, one book chapter, two books, and 27 patents. His main research areas are in high-efficiency power electronics conversions for high-power and energy applications.

Dr. Lai was the Founding Chair for 2001 IEEE International Future Energy Challenge (IFEC) and 2016 IEEE Asian Conference on Energy, Power and Transportation Electrification and the General Chair for IEEE Workshop on Computers in Power Electronics 2000, IEEE Applied Power Electronics Conference 2005, and IEEE Southern Power Electronics Conference 2018. He is also the General Chair for IEEE IFEEC 2019. He was the recipient of the Technical Achievement Award in Lockheed Martin Award Night, two journal paper awards, and 12 best paper awards from IEEE-sponsored conferences. He was also the recipient of the 2016 IEEE IAS Gerald Kliman Innovator Award. He led the student teams to win the Top Three Finalist in Google Little Box Challenge in 2016, Grand Prize Award from IFEC in 2011, and Grand Prize Award from Texas Instruments Engibous Analog Design Competition in 2009.

Gun-Woo Moon (S'92–M'00) received the M.S. and Ph.D. degrees in electrical engineering from the Korea Advanced Institute of Science and Technology (KAIST), Daejeon, South Korea, in 1992 and 1996, respectively.

He is currently a Professor with the Department of Electrical Engineering, KAIST. His research interests include modeling, design, and control of power converters, soft-switching power converters, resonant inverters, distributed power systems, power-factor correction, electric drive systems, driver circuits of plasma display panels, and flexible ac transmission systems.

Dr. Moon is a member of the Korean Institute of Power Electronics, Korean Institute of Electrical Engineers, Korea Institute of Telematics and Electronics, Korea Institute of Illumination Electronics and Industrial Equipment, and Society for Information Display.